IEEE Access
Multidisciplinary | Rapid Review | Open Access Journal

Received 23 September 2022, accepted 11 October 2022, date of publication 14 October 2022, date of current version 21 October 2022.

Digital Object Identifier 10.1109/ACCESS.2022.3214996

RESEARCH ARTICLE

Improved Performance of Hybrid PV and Wind Generating System Connected to the Grid Using Finite-Set Model Predictive Control

MAHMOUD F. ELMORSHEDY[1,2], (Member, IEEE), HABIB UR RAHMAN HABIB[3], (Senior Member, IEEE), MOSAAD M. ALI[4], M. JAGABAR SATHIK[1,5], (Senior Member, IEEE), AND DHAFER J. ALMAKHLES[1], (Senior Member, IEEE)

[1]Renewable Energy Laboratory, College of Engineering, Prince Sultan University, Riyadh 11586, Saudi Arabia
[2]Electrical Power and Machines Engineering Department, Faculty of Engineering, Tanta University, Tanta 31733, Egypt
[3]Department of Electrical Engineering, Faculty of Electrical and Electronics Engineering, University of Engineering and Technology Taxila, Taxila 47050, Pakistan
[4]Department of Electrical Engineering, Faculty of Engineering, Kafrelsheikh University, Kafr El-Shaikh 6860404, Egypt
[5]Department of Electrical and Electronics Engineering, SRM Institute of Science and Technology, Kattankulathur Campus, Kattankulathur, Tamil Nadu 603203, India

Corresponding author: Mahmoud F. Elmorshedy (mahmoud.elmorshedy@f-eng.tanta.edu.eg)

This work was supported by Prince Sultan University.

ABSTRACT This article proposes coordinated model predictive control (MPC) techniques for a DC-coupled hybrid microgrid system with solar photovoltaic and wind generated system. To achieve optimum power generation in the microgrid, the finite-control-set MPC (FCS-MPC) controls both PV-wind generated power using a DC-DC converter and a controlled rectifier. The mathematical formulation of the proposed hybrid microgrid system is described, and maximum power point tracking is employed to guarantee that the grid receives the maximum power. Furthermore, the 3-Φ bidirectional two-level inverter is connected between the DC-bus and AC grid which is controlled by the grid side FCS-MPC controller. The FCS-MPC is used in all system control parts, eliminating the use of four proportional controllers (PI) and giving a better dynamic response. Additionally, the outcomes are evaluated in comparison to current techniques. The proposed power management technique is also based on the relationship between the overall demand and the produced power provided by both WDG and PV sources. Due to the unpredictability of the sources, several scenarios, including (i) Fixed radiation and fixed wind speed, (ii) Wind speed variation and constant radiation, and (iii) Changing solar radiation and steady wind speed, are considered to validate the performance of the proposed scheme. The findings are then discussed.

INDEX TERMS Microgrid, model predictive control, coordinated control, energy management strategy, grid-connected systems, renewable energy resources.

NOMENCLATURE

AFE	Active front end.
ANN	Artificial neural networks.
CPL	Constant power load.
DMPC	Direct model predictive control.
EMS	Energy management system.
FCS	Finite control set.
HESs	Hybrid energy systems.
M.G.	Microgrid.
MPDPC	Model predictive direct power control.
PI	Proportional integral.
P&O	Perturb and observe.
PID	Proportional integral derivative.
PLL	Phase-locked loop.
PSF	Power signal feedback.

The associate editor coordinating the review of this manuscript and approving it for publication was Ahmed Mohamed.

PSO	Particle swarm optimization.
RERs	Renewable energy resources.
STC	Standard test conditions.
TSR	Tip-speed ratio.
VOC	Voltage-oriented control.
VSI	Voltage source inverter.
WGS	Wind generating system.
WT	Wind turbines.
SPV	Solar photovoltaic.

I. INTRODUCTION

The control of coupled power electronics converters has attracted a lot of attention in this decade. For example, with the use of solar photovoltaic, (PV) and wind generating system, (WGS) to produce renewable energy, power electronics converters are coupled in these supposed microgrids, such as [1], [2,], [3]. In the transportation section, another area of use for connected power electronics converters, such as those in [4], [5], [6], and [7], is the electrification of drive trains in conjunction with a battery as a form of energy storage. The mechanisms for charging, testing, or simulating batteries are often built on an effective AC-DC power electronics converter that provides power to one or more power electronics converters (such as DC/DC power converters), such as those found in [8] and [9]. Due to the large and quickly changing load power demands, controlling these power electronics converters is a complex operation. As a result, power converters that have sampling times of a few microseconds or less require extremely dynamic and reliable control methods. System limits must also be regularly considered in control to effectively operate and avoid damaging the power converters. The power converters of the coupled systems are commonly controlled by PI controller-based cascaded control structures. They cannot utilize knowledge regarding anticipated future states or preferred input behavior. They do not take system limits into account systematically.

MPC concepts, which are the emphasis of control concepts for power electronics converters control, can consider these factors [10], [11], [12], [13], [14]. They often do not consider other connected power converters because they are made to control just one power converter. As a result, the control of (extensive) interconnected systems is typically dependent on local decentralized control schemes, with no information being exchanged between the power converters, as seen in [1], [15], [16], [17], [18], and [19]. Without changing the overall control strategy, decentralized MPC techniques can be simply scaled up by adding more power converters and establishing quick data exchange amongst the power converters. As opposed to that, every modification to the load power or a power converter's setpoint causes an unidentified disruption in the neighboring power converters.

Furthermore, power converters often exhibit the CPL trend at their entry points. It poses a significant load behavior challenge for the components they supply and can significantly impair the stability of the complete coupled power converters system [20], [21]. To optimize the overall dynamics of the power converters and for financial reasons, it is preferred in order to minimize the size of these energy storage components. To overcome these problems, a mode-adaptive MPC approach in microgrids without data transfer is described in [17]. Compared to fixed control methods, this adaptive control scheme improves stability.

The system's overall control performance can be enhanced by either a centralized control technique or information sharing between the distributed controllers. A centralized FCS-MPC is proposed in [22] for a connected back-to-back power converter. According to the comparison, a centralized approach works better than a PI-based DMPC. In this study, there is one step ~~of~~ the prediction horizon. The authors in [23] provide an expansion to two prediction horizons. The authors in [24] present a centralized MPC for AC/DC power converters that operate in parallel. These centralized MPC techniques have relatively small prediction horizons, which means that known future behavior (such as setpoints) cannot be fully utilized. For (big) interconnected systems, centralized techniques typically fall short of real-time requirements in a few microseconds. Finally, when there are more connected systems, the computing effort rises dramatically.

Some of these problems can be avoided by using coordinated MPCs integrated into EMS. Here, simply a data link is provided to enable the coordinated MPC techniques, while several MPC techniques locally regulate power converters, such as [25], [26], [27], and [28], to share the projected future trends. This kind of MPC approach is primarily used in power plant systems and microgrid applications [29], [30], [31]. These systems typically have substantially lower dynamics and employ sample rates in the region of one second compared to connected power converters. For AC/DC-link systems, the authors in [32] compare a coordinated MPC, a centralized MPC, and a PID control based on PSO. The comparison demonstrates that the coordinated MPC has significant advantages over the centralized MPC in practical implementation and outperforms PID-based techniques for controlling interconnected systems. This application used a fifty-step prediction horizon and a ten-millisecond sample period. An FCS-MPC with a prediction horizon of two steps is the foundation of the coordinated MPC technique for a back-to-back converter introduced in [33]. The active front end (AFE) rectifier and inverter MPCs communicate the anticipated condition and potential switching combinations. One may attain a sampling time of one hundred microseconds.

Rule-based and optimization-based control techniques are the two categories under which EMS systems are typically categorized [29], [30], [31], [32], [33]. Direct or fuzzy rules are used in rule-based techniques to allocate the required amount of electricity among the various energy sources. The hybrid system's power characteristics or optimization methods can be used to derive the rules in these methods [32]. These EMS systems are reliable, do not rely on actual performance, and can effectively distribute power across

diverse energy sources by utilizing a straightforward strategy. These methods are appropriate for real-time control applications [29], [30], [31], [32], [33]. Reference values are obtained in optimization-based techniques in accordance with the improvement of a momentary cost function. These approaches require significant computing effort and are complex, which influence the EMS systems' response [33].

The authors of [34] have proposed a distributed EMS based on a hybrid system's rule-based approach. The energy storage devices' power capability, remaining capacity, and demand power are all factors that the suggested EMS in this study considers. In [21], a rule-based EMS is set up to guarantee the proposed system's reliable performance in a variety of AC microgrid operating modes. The solution performs better and is simpler than the conventional cascade control method.

A thorough analysis of HES is provided in [35], which includes an overview of the many configurations and classifications of HES and information on optimization, storage, and size. The numerous configurations and combinations of HES, the kinds of converters utilized, as well as certain control mechanisms, a crucial component of HES, HES size, and HES' energy management under various scenarios, the various types of energy systems and their parts are all covered.

Based on the coordinated MPC approach, this study presents an EMS system for a DC-coupled hybrid grid-connected PV/WGS microgrid. The recommended DC-coupled hybrid MG configuration and controller scheme is shown in Fig. 1. The recommended configuration has two power sources: solar PV and WGS. The proposed control approach is divided into two parts: controllers at the device and system levels. A coordinated MPC control strategy with the solar PV control unit, WGS control block, and DC/AC power converter control block is described for device-level controllers. A centralized control unit (EMS) for communication between multiple device-level control blocks and optimized power distribution among various power sources are also included in the system-level control. In line with the working limits of individual sources, the EMS produces the proper set values for controlling the current and the power of DC-DC and DC-AC converters, respectively. Additionally, a WGS rectifier control is employed to extract the maximum power. It is also important to note that all controllers are developed using an MPC technique.

Consequently, the following are the primary contributions of this study:

- A complete model is developed to determine the solar output and the MPPT characteristics.
- Three power converters are developed: (i) a DC/AC bi-directional grid-connected inverter, (ii) a DC-DC converter for solar PV, and (iii) a controlled rectifier for the WGS generating system.
- To control the AC/DC converter, the MPDPC technique aims to achieve a faster dynamic response and reduce ripple. The adopted strategy is further validated through simulation data with conventional methods.

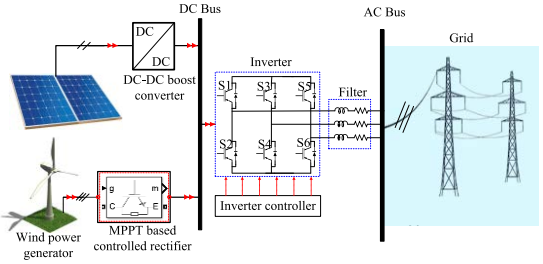

FIGURE 1. Schematic diagram of the developed HMGES.

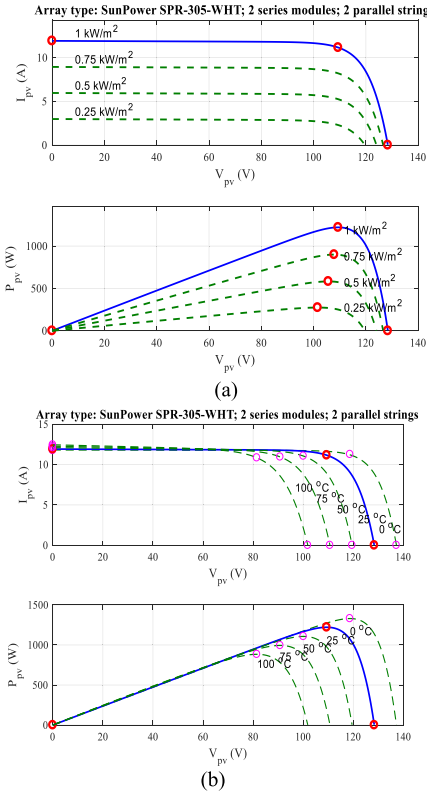

FIGURE 2. Effects of temperature and solar radiation on the power of a PV system. (a) variable solar radiation and (b) variable temperature.

- A coordinated MPC technique is implemented for the regulation of power and current of AC-DC and DC-DC converters, respectively.
- An EMS method is applied to create the appropriate set points per each power source's operational objectives.

II. MATHEMATICAL MODELLING OF THE PROPOSED SYSTEM

In this work, the suggested hybrid renewable energy system (HRES) consists of three main components: PV array, WGS, and beside grid, as demonstrated in Fig. 1. Each component in the hybrid microgrid energy system (HMGES) has its control unit with specific functions during different conditions. The following subsections discuss the mathematical representation of each component as well as the technical and financial specifications.

TABLE 1. Technical and economic specifications of the SunPower305SPR SPV module.

Parameter	Amount	Parameter	Amount
Efficiency at STC	13%	Rated capacity per module	305 W
Open circuits voltage per-module	64.200 V	Nominal operating temperature	46°C
Short circuits current per-module	5.960 A	Temperature coefficient	-0.386 % per °C
MPP voltage per-module	54.700 V	Working temperature scale	(-40 ~ +85)◦C
MPP current per-module	5.580 A	Lifetime	25 years
Derating factor	85%	Capital cost	1000 $/kW

TABLE 2. Technical specification of the WECS.

Parameters	Amount	Parameters	Amount
Inertia	0.2 kg.m2	PMSG rated speed	211 rpm
Rated torque	905 Nm	Stator inductance	4.48 mH
Stator resistance	0.1764 Ω	Typical wind speed	12 m/s
Rated capacity	20 kW	Rotor diameter	5 m

A. MATHEMATICAL REPRESENTATION OF THE PV PANEL

PV array is one of the principal sources of renewable energy in the developed HMGES. The proposed study employs a monocrystalline silicon flat plat SunPower-305-SPR SPV model with a typical rating of 305 Watt and 13% efficiency. Table 1 demonstrates the technical specs of individual modules of the employed SPV according to the manufacturing data [36]. The module output power and efficiency are determined according to two main factors: the working temperature and solar radiation. Accordingly, the PV output power, efficiency, and the actual PV cell temperature can be expressed by [37] and [38]

$$P_{PV} = f_{PV} P_{PVn} \left[1 + \beta_r (T_{PV} - T_{PV,STC})\right] \times \left(\frac{G_T}{G_{T,STC}}\right) \quad (1)$$

$$\eta_{PV} = \eta_{T_{STC}} \left[(1 - \beta_r (T_{PV} - T_{STC})) + \gamma log_{10}(G_T)\right] \quad (2)$$

$$T_{PV} = (T_{NOCT} - 20)\left(\frac{G_T}{G_{T,STC}}\right) + T_{air} \quad (3)$$

where, T_{PV} is the actual temperature, T_{air} is the ambient temperature, $T_{PV,STC}$ is the temperature of the PV cell at STC, and T_{NOCT} is the nominal operating temperature. Meanwhile, G_T is the PV array's average hourly solar radiation at the recommended working temperature, $G_{T.,STC}$ represents the solar radiation (SR) at STC (1 kW/m^2). In addition, η_{SPV} represents the efficiency measured at STC, P_{PVn} represents nominal power, and γ SR is the intensity coefficient for the solar cell efficiency. The effect of these two factors on the generated power is shown in Fig. 2-a and b.

B. MATHEMATICAL REPRESENTATION OF WIND GENERATING SYSTEM

WT is coupled to PMSG in the WDG system. A controlled rectifier changes AC into DC power, which is used to control the generated power. The technical details of the WT under investigation are provided in Table 2 [39]. The amount of WT-generated power is determined according to different parameters, as expressed in (4). Concurrently, one can determine the generated WT power as a function of the turbine coefficients and wind speed, as mentioned in Eq. (5) [40].

$$\boldsymbol{P}_{WT,r} = 0.5\boldsymbol{A}\boldsymbol{\rho}\boldsymbol{V}\omega_d{}^3\eta_{\mathrm{WT}}\eta_{\mathrm{PMSG}}\boldsymbol{C}_p(\boldsymbol{\beta}, \boldsymbol{\lambda}) \quad (4)$$

$$P_{W.T} = \begin{cases} P_{W.T,r}\left(\frac{V_{\omega.d} - V_{c.i}}{V_r - V_{c.i}}\right) & if\ V_i < V_{\omega.d} < V_r \\ P_{W.T,r} & if\ V_r \le V_{\omega.d} < V_o \end{cases} \quad (5)$$

C. MATHEMATICAL MODEL OF THE GRID AND ITS SPECIFICATIONS

Generally, the interconnecting converter is employed to exchange power between AC and DC MG systems. The prime power converter (PPC) was modelled generically. According to [41], the PPC rating should be greater than the power generated from combined AC and DC sides, as described by

$$N_{conv} \ge \eta_{AC/DC}.P_{WT}(t) + \eta_{DC/AC}.P_{PV}(t) \quad (6)$$

where N_{conv} is the converter size in kW, $\eta_{AC/DC}$ represents the efficiency of the AC to DC converter, and $\eta_{DC/AC}$ represents the efficiency of the DC to AC converter.

III. PROPOSED CONTROL STRATEGIES FOR SYSTEM COMPONENTS

In this section, the details control methods for all systems and converters will be discussed.

A. MPPT OF PV ARRAY

The PV-generated power and efficiency decrease during high temperatures, although the high levels of PV radiation increase these two factors. The solar output voltage at the peak power point (V_{mpp}) must be maintained even when the temperature and radiation change. MPPT methods could be used to accomplish this, as investigated in many articles. The MPPT techniques are separated into two main categories; the direct techniques include incremental conductance (IC), perturbation and observation (P&O), as well as sophisticated methods like ANN and fuzzy logic-based schemes [42], while the indirect techniques, like the short-circuit and open-circuit methods [43], [44]. Due to the requirement for a prior understanding of the PV's operating characteristics, it is difficult to accurately monitor the MPP using indirect techniques at any cell temperature or solar radiation [45]. Conversely, in the direct methods, the voltage levels of both PV and DC-bus are controlled through by moderating the signal used as a DC-DC converter's reference. The main features of utilizing P&O or IC methods are their compatibility with digital controllers and industrial inverters, no prior knowledge is

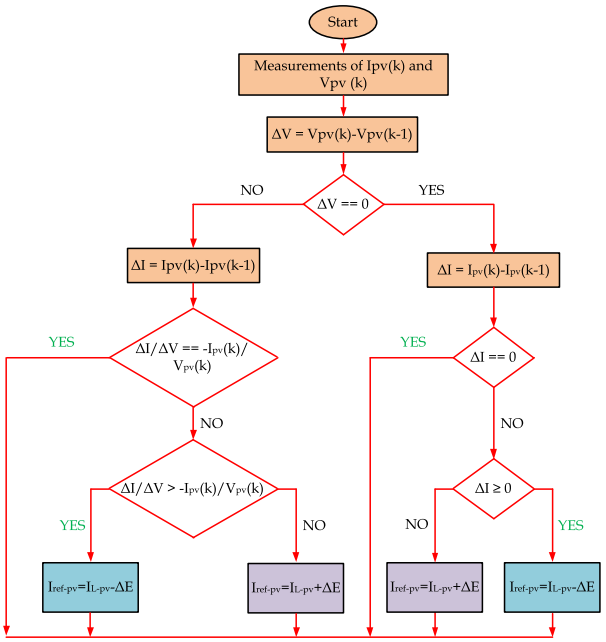

FIGURE 3. Flowchart of the incremental conductance (IC) method for the MPP extraction.

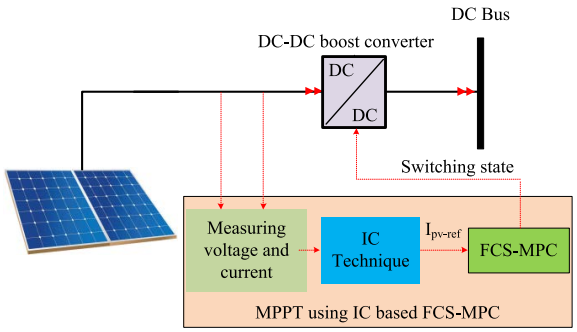

FIGURE 4. The MPPT uses IC-based FCS-MPC.

needed about the PV, and their reduced cost [46]. The main limitation ~~in~~ of the P&O method is the voltage oscillation during transient changes in weather conditions. In contrast, the IC method improves tracking speed and accuracy problems [42]. The main advantages of using intelligent techniques over direct ones are their improved tracking speed and precision, nonetheless their complexity and expensive application costs. [47]. In this context, the IC method can be combined with a direct control method to enhance the system characteristics [48].

Hence, in this paper, the IC technique is combined with the MPC to perform the MPPT operation for the PV system. Firstly, the IC is used to generate the optimum current from the PV, I_{ref_PV} achieved by the MPP. Figure 3 demonstrates the flowchart of the IC algorithm. The working principles of this IC technique start from measuring the generated PV output current and the voltage. Then, differentiate the time, and the obtained values are compared to zero. Depending on the output voltage and current sign, the value of the I_{ref_PV} is

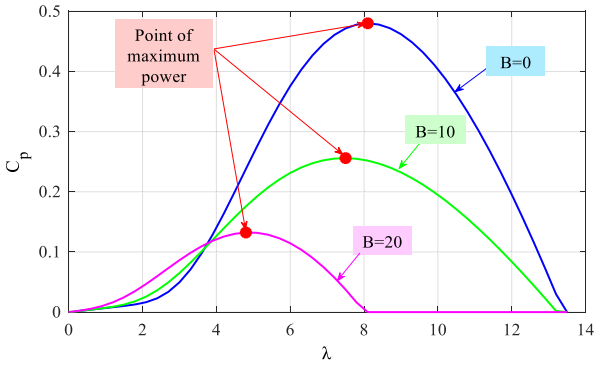

FIGURE 5. The (Cp-λ) characteristics at several pitch angles β.

updated using the incremental value ΔE, which is a trade-off between the power oscillation and the speed of tracking the MPP. Then, this optimum current is fed to the MPC to control the ON/OFF states of the DC-DC converter. To use the MPC, the discrete model for the DC-DC converter state, i_L, is needed to be defined to predict the next step. As mentioned, there are two possible switching states, 1 or 0. Based on the switching states and Euler discretization rule for the dynamic model of the DC-DC boost converter, the predicted value of the inductor current, $i_L(k+1)$, which equals the PV output current, is calculated by

$$i_L\,(k+1) = i_L\,(k) + \frac{T_s}{L}\left(V_{pv} + V_{DC}\,(k) \bullet (S-1)\right) \quad (7)$$

where k and $(k+1)$ are the current and next instant, respectively. S is the switching state 1 or 0. V_{pv}, T_s, V_{DC} are the PV output voltage, the sampling time, and the DC-bus voltage. The value of this predicted current $i_L(k+1)$ changes based on the switching state. Hence, to generate the MPPT, the switching state is calculated, which is chosen to minimize the error between the predicted input DC-DC boost converter current and the reference derived from the IC method. This cost function is given by

$$g = \left|i_L\,(k+1) - i_{ref-pv}\right| + I \quad (8)$$

where I is the penalty function which is used to prevent the PV array from damage and is determined by

$$I = \begin{cases} \infty & \text{if } I_{sc}\,(k+1) > I_{sc} \\ 0, & \text{otherwise} \end{cases} \quad (9)$$

The schematic diagram is demonstrated in Fig. 4 displays the MPPT control of the PV array. The PI control is employed to improve the tracking accuracy by damping the ripple oscillation and enhancing the computation accuracy.

B. MPPT FROM THE WGS

There are three categories: WT fixed speed, variable speed with pitch control, and full-controlled variable speed [49]. DFIG and PMSG have been widely used in WDG systems due to their ability to realize maximum power and wide speed control operation [50]. The MPPT methods reported

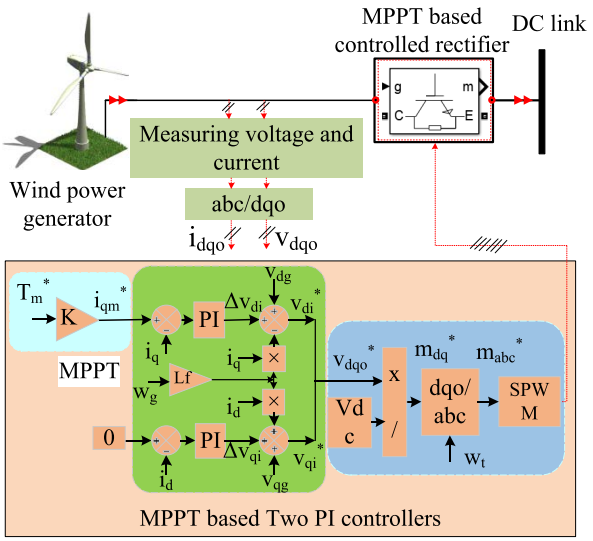

FIGURE 6. MPPT control from the WGS is based on two PI controllers.

in the literature for variable speed WTs are classified into PSF, P&O, and wind speed measurement (WSM). In the PSF technique, the MPP is tracked by shaft speed control, and the controller must be provided with the maximum power curve. [51]. The P&O technique has excellent reliability but ineffective efficiency. In the P&O technique, No prior knowledge of the maximum WT power at different wind speeds or generator data is required [52]. The WSM technique involves two feedback signals: the wind and the turbine speeds for calculating the TSR. So this technique is known as the TSR as well [53]. In the above MPPT techniques, the WT is pushed to stop operating when the output power exceeds the rated power during working above the recommended wind speed. For this purpose, the pitch angle control (PAC) is applied for the variable speed turbine to keep the WT generating the rated output power and reduce the overloading [49], [54]. The blade PAC can be accomplished using different controllers such as (PI, PID, sliding mode control, fuzzy logic control (FLC), FLC-PI, and FLC-PID) [55]. One of the main limitations of implementing conventional controllers is the need to accurately determine the controller gains to ensure robust operation [54], [55].

In this work, the PMSG is adopted, where the dynamic model is constructed using MATLAB/Simulink software in the *dq*-synchronous frame. Meanwhile, the following formulations are used to represent the wind power coefficient of the WT [56], [57]:

$$C_p(\beta, \lambda) = C_a\left(\frac{C_b}{\lambda_i} - C_c - C_d\beta\right)e^{\frac{C_f}{\lambda_i}} + C_g\lambda \tag{10}$$

$$\lambda = \frac{\omega_r R}{V_{\omega d}}, \quad \lambda_i^{-1} = \frac{1}{0.08\beta + \lambda} - \frac{0.035}{\beta^3 + 1} \tag{11}$$

where $C_a = 0.51760$, $C_b = 116.0$, $C_c = 5.0$, $C_d = 0.40$, $C_f = 21.0$ and $C_g = 0.00680$. λ is the TSR, R represents the blade radius, and $V_{\omega d}$ the wind speed. The relation between C_p and λ at various blade pitch angles, β is presented in Fig. 5.

The observation is that at a specific value of β, the maximum point of C_{p-opt} exists at only one value of λ_{opt}.

In this paper, the TSR is adopted to extract the MPP from the WGS, where two control methods can be used. The first one employs two cascaded PI controllers, while the second uses FCS-MPC to generate the control signals for the controlled rectifier. More details about each method are given in the following sub-sections.

1) MPPT-BASED TWO PI CONTROLLERS

As mentioned before, the controlled rectifier is used instead of the switch-mode rectifier; hence the controller algorithm is different. Using the PMSG's dynamic model as a foundation, the *dq*-axis currents are used for control, where both can achieve a separate objective. The *q*-axis reference current value is used to extract the maximum power, whereas the *d*-axis is used to reduce the losses. The reference *q*-axis reference current, i_{qs}^* is obtained based on the optimum wind power, P_{opt}, and it can be given out by [58]

$$i_{qs}^* = \frac{2}{3}\frac{2}{p}\frac{1}{\lambda_m}\frac{P_{opt.}}{\omega} \tag{12}$$

The optimum wind power, P_{opt}, can be calculated from:

$$P_{opt.} = 0.5 \times C_{p-otp.} \times \rho \times A \times V_w^3 \tag{13}$$

The optimum power is extracted for the investigated WT parameters at a tip-speed ratio of 8.1, which corresponds 0.48 wind power coefficient [59]. On the other hand, the reference point of the *d*-axis current is adjusted to zero, $i_{ds}^* = 0$, to reduce the power losses [60]. After determining the *dq*-axis reference values, both *dq*-axis current references (i_{ds}^*, i_{qs}^*) are compared with their measured values. Subsequently, two PI controllers are utilized to ensure the actual values track their references fine. Furthermore, the compensation is used to get a complete decoupling. Finally, the controlled rectifier pulses are obtained based on the compensated output from the two PI controls and then converted to *abc* references. Fig. 6 shows the MPPT control from the WGS-based two PI controllers.

2) MPPT BASED FCS-MPC

The FCS-MPC is employed instead of the PI control for faster transient and better dynamic responses to extract the MPPT. Using the FCS-MPC for the controlled rectifier has many advantages over the PI controller, such as removing two PI controllers, and hence four tuning gains can be avoided. Besides removing the pulse width modulation techniques. Moreover, selecting the best switching vector gives a minimum cost function value.

The FCS-MPC can be elaborated into three essential steps to optimizing its efficiency. The first step is to measure the desired states. Then the prediction condition comes next, and finally, the control variable is optimized using the desired cost function. The best switching voltage vector is selected based on the cost function minimization. The mathematical details of the FCS-MPC are as follows:

- Measuring the rotating speed, and stator currents

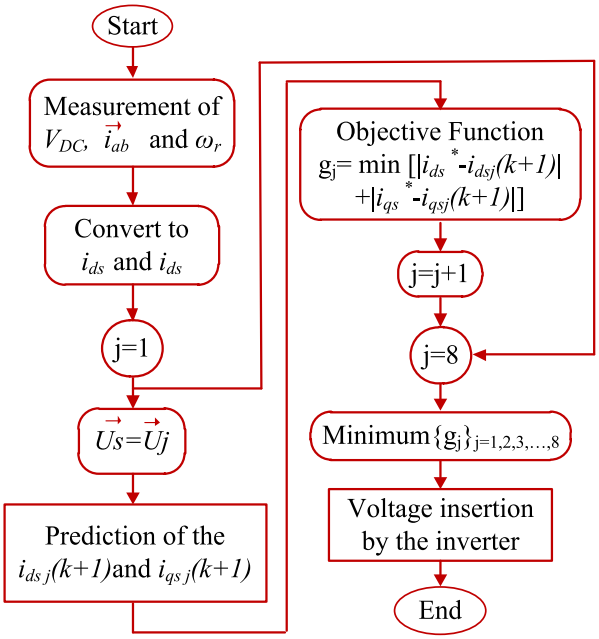

FIGURE 7. Flowchart of the proposed FCS-MPC for the controlled rectifier.

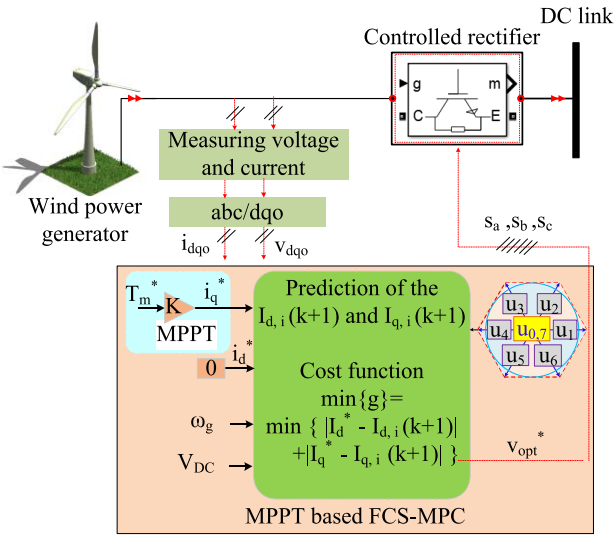

FIGURE 8. MPPT control from the WGS based on FCS-MPC.

- Predicting the dq-axis currents, $i_d(k+1)$, $i_q(k+1)$, with the help of the first-order Euler method as follows [61]

$$I_{d,i}(k+1) = I_d(k) + T_s\left(\frac{u_{d,i}(k)-I_d(k)\times R_s}{L_d} + \omega_e \times I_q(k)\right) \quad (14)$$

$$I_{q,i}(k+1) = I_q(k) + T_s\left(\frac{u_{q,i}(k)-I_q(k)\times R_s-\omega_e\times\psi}{L_q} + \omega_e \times I_d(k)\right) \quad (15)$$

$I_q(k)$ and $I_d(k)$ represent the dq-axis actual currents, Ψ represents the permanent magnet flux linkage, and ω_e represents the electrical rotating speed.

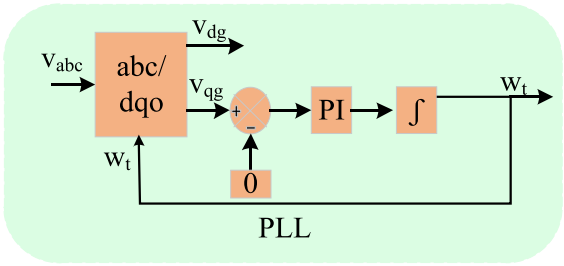

FIGURE 9. The block diagram of PLL technique.

- Design of the proposed cost function, g as given by

$$g = \left|I_{ds}^{*} - I_{ds,i}(k+1)\right|^2 + \left|I_{qs}^{*} - I_{qs,i}(k+1)\right|^2 + W \quad (16)$$

wehere W is the current limitation to protect the machine from overcurrent, the wrong switching vector can be directly avoided. This current limitation can be determined by

$$W = \begin{cases} \infty & \text{if } \sqrt{{I_{ds}}^2(k+1) + {I_{ds}}^2(k+1)} > I_{\max} \\ 0, & \text{otherwise} \end{cases} \quad (17)$$

The observation is that the cost function does not require the weighting factor. Meanwhile, the reference values for the dq-axis current are inserted directly into the cost function. The flowchart of the applied FCS-MPC for the controlled rectifier is demonstrated in Fig.7. Moreover, the overall Machine side rectifier controller based on the FCS-MPC for maximum power extraction is illustrated in Fig. 8.

C. GRID SIDE CONVERTER CONTROL

It is critical to match the generated voltage and frequency to the grid requirements. Thus, equipping the three-phase VSI with a specific controller is mandatory. This controller contains three parts phase-locked loop control, DC-bus voltage controller, and grid current controller. Details of each controller will be discussed in the following subsection.

1) PHASE-LOCKED LOOP

The main target of the PLL is to extract the grid voltage angle for proper alignment of the d-axis with the voltage vector in the VOC [15]. Based on the VOC principles, the q-axis grid voltage is adjusted to zero ($v_{qg} = 0$). The PLL function is to keep the d-axis of the grid voltage with respect to the voltage vector, and hence the q-axis voltage is formulated by

$$v_{qg} = \hat{v}_{ph1}\sin(\omega t_o - \omega t) \quad (18)$$

where, ωt_o represents the angle of the voltage vector and ωt the angle of the d-axis. Both angles are measured with respect to α-axis. The diagram of the PLL technique is illustrated in Fig. 9.

2) DC-BUS VOLTAGE CONTROL

The DC-bus voltage is constantly maintained by regulating the grid d-axis current. This is illustrated based on the input-output power balance and considering the system is lossless

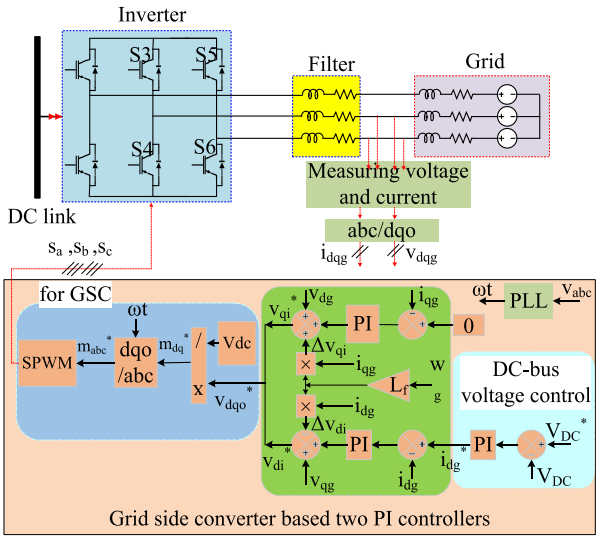

FIGURE 10. Grid side inverter controller, including the DC-link voltage controller based on PI controllers.

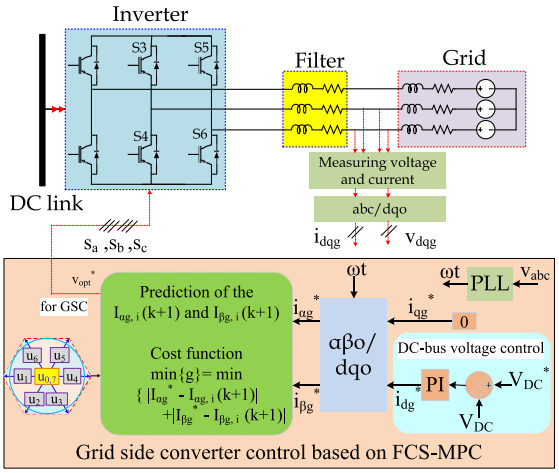

FIGURE 11. Grid side inverter controller, including the DC-link voltage controller based on FCS-MPC.

as given by [62]

$$\frac{3}{2}\left(v_{qg}i_{qg}+v_{dg}i_{dg}\right)=C.v_{dc}.\frac{dv_{dc}}{dt} \tag{19}$$

Based on the principle of the VOC where $v_{qg}=0$ and $v_{dg}=v_{ph1}$ Eq. (19) can be modified to

$$\frac{3}{2}v_{dg}i_{dg}=C.v_{dc}.\frac{dv_{dc}}{dt} \tag{20}$$

This equation can be rewritten after taking linearization around the equilibrium point to

$$\frac{3}{2}\hat{v}_{dg}I_{dg}+\frac{3}{2}V_{dg}\hat{i}_{dg}+\frac{3}{2}V_{dg}I_{dg}+\frac{3}{2}\hat{v}_{dg}\hat{i}_{dg}=C.V_{dc}.\frac{dv_{dc}}{dt} \tag{21}$$

where $\hat{v}_{dg}$ and $\hat{i}_{dg}$ are the perturbation in the d-axis voltage and current, respectively. By neglecting the steady-state and higher-order terms, results it can be written by

$$\frac{3}{2}\hat{v}_{dg}I_{dg}+\frac{3}{2}V_{dg}\hat{i}_{dg}=C.V_{dc}.\frac{dv_{dc}}{dt} \tag{22}$$

It is evident that the magnitude of the DC-bus voltage varies according to the value of the d-axis output current. Thus, it uses a PI control technique to regulate the DC-bus voltage.

3) GRID CURRENT CONTROL (GCC)

After generating the reference d-axis current from the DC-bus voltage control loop and selecting the reference value of the q-axis current to achieve unity or leading or lagging power factor. The grid current control can be designed. In this work, the GCC can be designed based on two methods, the first one depends on the application of two PI controls, and the second is based on the FCS-MPC. More analyses about each method are in the following.

a: GCC BASED ON PI CONTROLLERS

The dq-axis output voltages from the inverter can be expressed by [63]

$$v_{di}=v_{dg}+R_f i_{di}+L_f p i_{di}-\omega_f L_f i_{qi} \tag{23}$$
$$v_{qi}=v_{qg}+R_f i_{qi}+L_f p i_{qi}+\omega_g L_f i_{di} \tag{24}$$

where ω_f represents the grid angular frequency, R_f, L_f are the filter resistance and inductance. These two equations can be rewritten by

$$v_{di}=\left[R_f+L_f p\right]i_{di}+v_{dg}-\omega_f L_f i_{qi} \tag{25}$$
$$v_{qi}=\left[R_f+L_f p\right]i_{qi}+v_{qg}+\omega_g L_f i_{di} \tag{26}$$

The effects of filter values can be replaced by PI controllers as in the following relations.

$$\begin{aligned}v_{di}^{*}&=PI_{i_{di}}\left[i_{di}^{*}-i_{di}\right]+v_{dg}-\omega_f L_f i_{qi}\\&=\Delta v_{di}+v_{dg}-\omega_f L_f i_{qi}\end{aligned} \tag{27}$$
$$\begin{aligned}v_{qi}^{*}&=PI_{i_{qi}}\left[i_{qi}^{*}-i_{qi}\right]+v_{qg}+\omega_f L_f i_{di}\\&=\Delta v_{qi}+v_{qg}+\omega_f L_f i_{di}\end{aligned} \tag{28}$$

From the above equations, it could be observed that the dq-axis output currents are regulated by adjusting the dq-axis voltages of the inverter (v_{di}, v_{qi}). As mentioned before, the DC-bus voltage control loop achieves the reference value of the d-axis current. Meanwhile, the q-axis reference current is kept to zero to obtain a unity power factor. Voltage compensation removes the coupling between the d- and q-axis. The block control diagram, including the pulses generation, is illustrated in Fig. 10.

b: GCC BASED ON FCS-MPC

The FCS-MPC is used to overcome the slow dynamic response, more time for tuning gains, and the complex process of generating the pulses to the VSI when PI controllers are used. The FCS-MPC is easier, simpler, and has faster

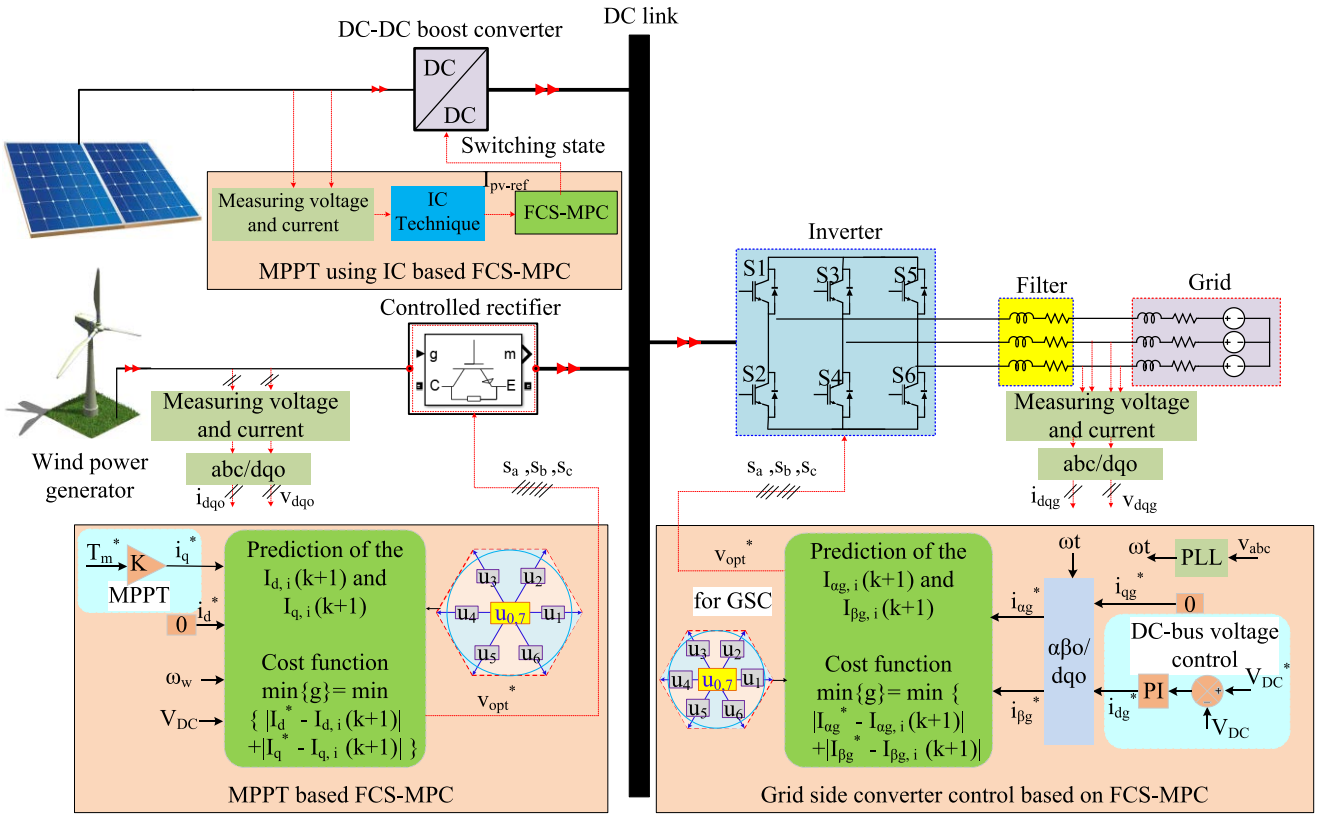

FIGURE 12. Complete the block diagram of the HRES connected to the grid using the FCS-MPC.

dynamic responses. Based on the stationary reference frame, the $\alpha\beta$-axis current can be predicted as follows

$$I_{\alpha,i}(k+1) = I_{\alpha}(k) + T_s\left(\frac{u_{\alpha,i}(k) - u_{\alpha}(k) - I_{\alpha}(k) \times R_f}{L_f}\right) \quad (29)$$

$$I_{\beta,i}(k+1) = I_{\beta}(k) + T_s\left(\frac{u_{\beta,i}(k) - u_{\beta}(k) - I_{\beta}(k) \times R_f}{L_f}\right) \quad (30)$$

Then the cost function can be implemented as follows

$$g_g = \left|I_{\alpha}^{*} - I_{\alpha,i}(k+1)\right|^2 + \left|I_{\beta}^{*} - I_{\beta,i}(k+1)\right|^2 + W \quad (31)$$

The schematic of the grid side inverter based on the FCS-MPC is shown in Fig. 11.

IV. PROPOSED ENERGY MANAGEMENT STRATEGIES

Due to the fluctuating nature of RERs, the optimal output power can be higher or lower than the required load demand. Accordingly, the proposed energy management strategy (PEMS) is employed to improve the HRES system performance under various conditions. The schematic diagram shown in Fig. 12 demonstrates the hybrid system components incorporated with their individual controller. The main objectives of the PEMS are:

TABLE 3. Grid side converter controller gains.

Controller name and type	DC-link voltage	D-axis current	Q-axis current
Value of proportional, Kp	0.5	$1.921\text{x}10^2$	$1.921\text{x}10^2$
Value of integral, Ki	5.0	$9.767\text{x}10^4$	$9.767\text{x}10^4$

TABLE 4. Machine side converter controller gains.

Controller name and type	D-axis current	Q-axis current
Value of proportional, Kp	100	250
Value of integral, Ki	100	200000

TABLE 5. Machine side converter controller gains.

Type	Value
Proportional, Kp	0.051
Integral, Ki	1.0

- Extracting the optimal power from each generating unit by utilizing MPPT techniques to the WDG and the PV array.
- Organizing the total produced power across all generating units.

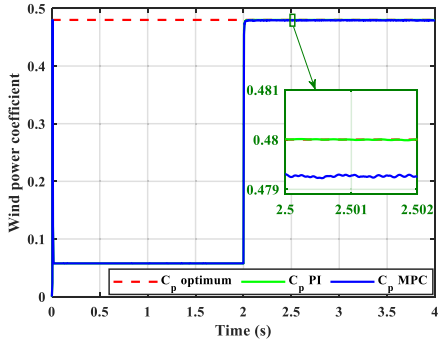

FIGURE 13. Optimum and actual wind power coefficient during case 1 using MPC and PI based SVM.

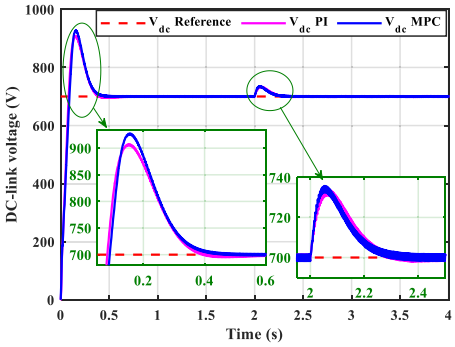

FIGURE 14. Reference and actual DC-link voltage response during case 1 using MPC and PI based SVM.

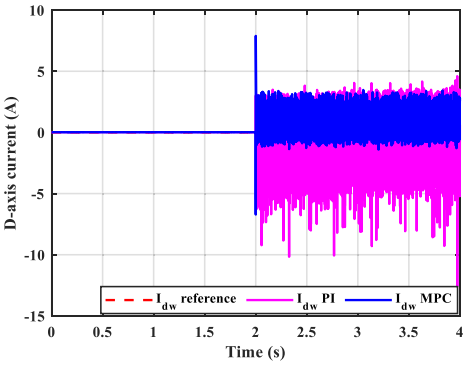

FIGURE 15. Reference and actual D-axis current generated from the WGS during case 1 using MPC and PI based SVM.

- Maintaining the DC-link voltage to a constant magnitude during different sudden disturbances.
- Injecting the extracted power into the grid achieves the unity power factor and synchronizes the voltage magnitude and frequency with the grid requirements.

V. TECHNICAL EVALUATION USING THE PROPOSED HMGES BASED ON MODEL PREDICTIVE CONTROL

This section presents the optimized system's technical evaluation developed using MATLAB/Simulink. The optimal HMGES parts were formulated in MATLAB/Simulink with the ratings listed in Table 1 and 2. The technical analysis has three basic objectives: achieving effective management between key system components; ensuring uninterrupted, continuous, consistent voltage and frequency feeding of the

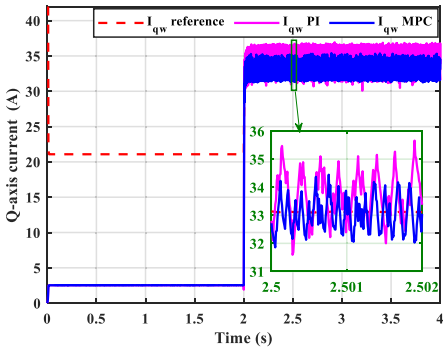

FIGURE 16. Reference and actual Q-axis current generated from the WGS during case 1 using MPC and PI based SVM.

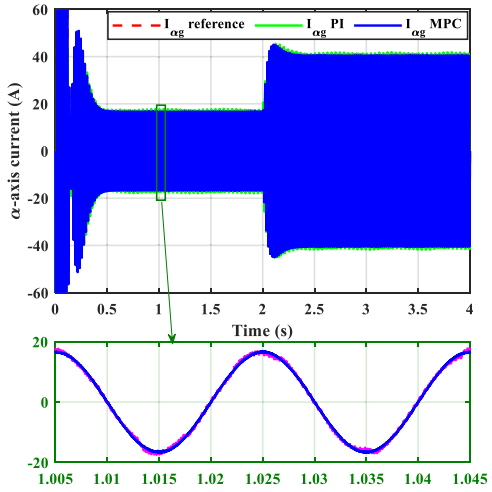

FIGURE 17. Reference and actual α-axis current injected into the grid during case 1 using MPC and PI based SVM.

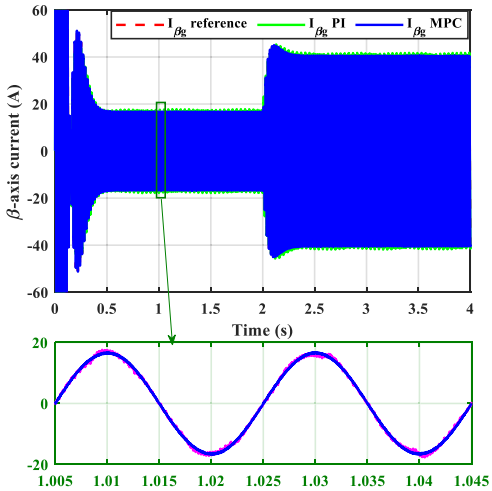

FIGURE 18. Reference and actual β-axis current injected into the grid during case 1 using MPC and PI based SVM.

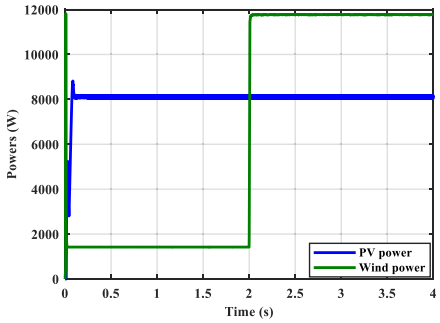

FIGURE 19. Optimum generated power from PV and WG systems at case 1.

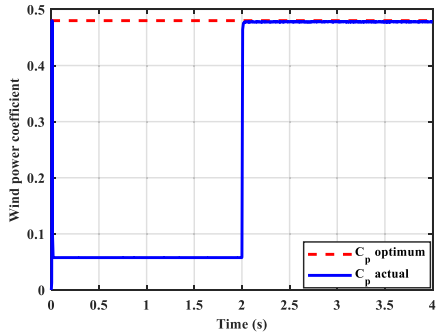

FIGURE 20. Optimum and actual wind power coefficient during case 1.

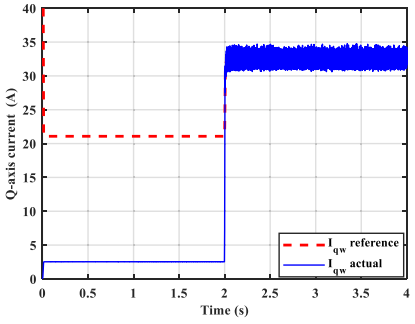

FIGURE 21. Reference and actual Q-axis current generated from the WGS during case 1.

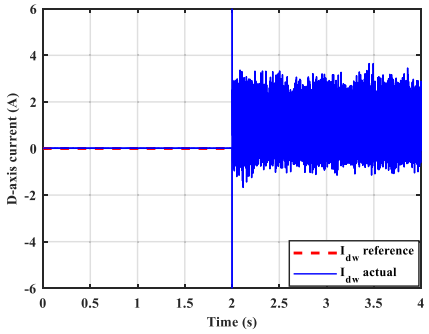

FIGURE 22. Reference and actual D-axis current generated from the WGS during case 1.

loads; and maintaining the voltage at the dc-bus under various conditions. It should be noted that until the generated

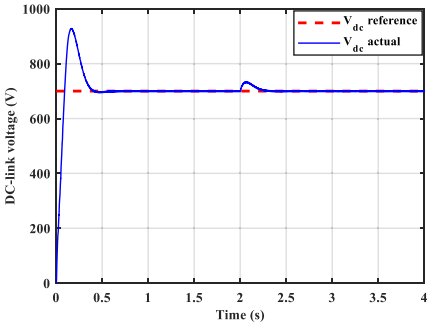

FIGURE 23. Reference and actual DC-link voltage response during case 1.

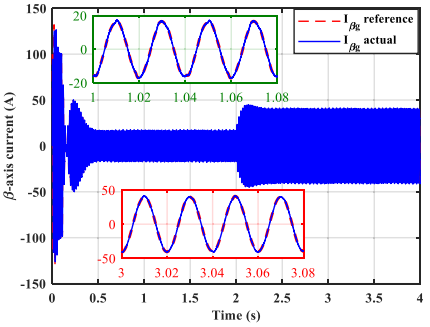

FIGURE 24. Reference and actual α-axis current injected into the grid during case 1.

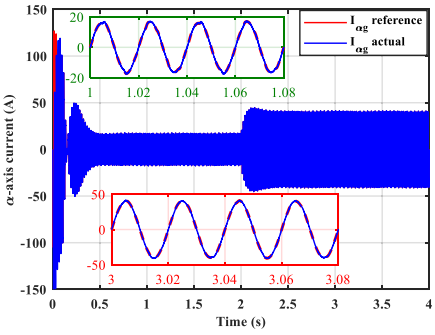

FIGURE 25. Reference and actual β-axis current injected into the grid during case 1.

voltage reaches its steady-state value, which is discovered after 5 seconds, the WDG is regarded as starting at no load. In other words, the loads are first supplied by the SPV array and the batteries (if necessary).

The four seasons of the year were examined using technical analysis in the following ways:

The technical evaluation is implemented using the MATLAB/Simulink environment. The capacities listed in Tables A1 and A2 were used to construct the HMGES components in MATLAB/Simulink. The technical analysis has three objectives: (i) achieving effective management between system components, (ii) ensuring maximum power from renewable sources, and (iii) all generated power is supplied to the grid by maintaining unity power factor and constant voltage at the DC-bus irrespective of loading condition. It should

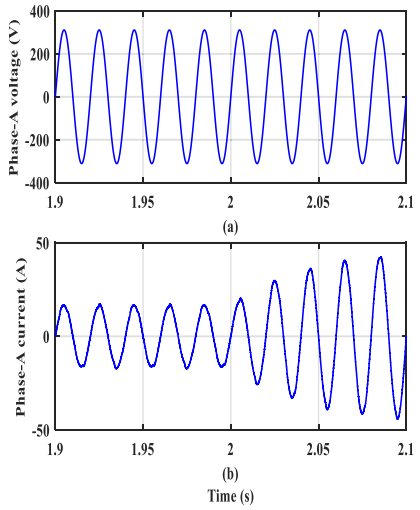

FIGURE 26. Simulation results of the main grid during case 1. (a) Phase-A voltage, and (b) Phase-A current.

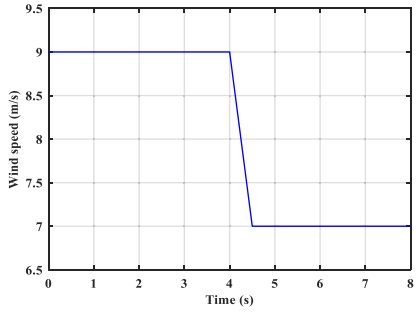

FIGURE 27. Profile of wind speed variation.

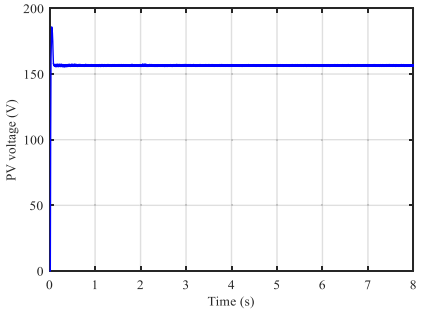

FIGURE 28. PV panels output voltage.

be noted that the WGS supplies the generated power after 2 seconds until the generated voltage reaches its steady-state value, where it starts at no load. In other words, the grid is first connected by the SPV array. Technical evaluation is analyzed under four different cases as follows:

A. CASE 1 COMPARATIVE ANALYSIS OF THE OUTCOMES BETWEEN MPC AND CONTEMPORARY PI BASED SVM

In this case, the performance comparison for the overall system using the MPC and the PI controller-based SVM is presented. Due to the use of the SVM in the grid side converter and the machine side converter, the presented results

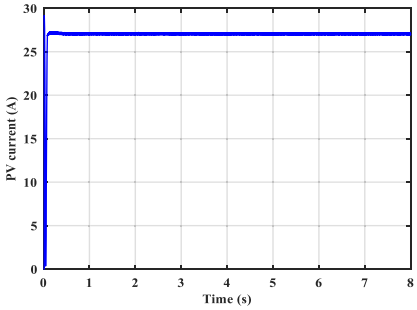

FIGURE 29. PV panels output current.

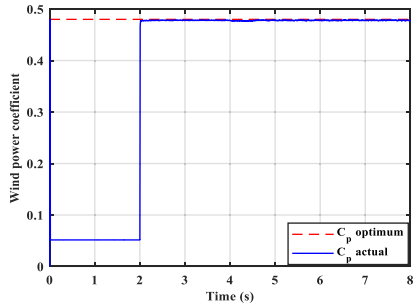

FIGURE 30. Optimum and actual wind power coefficient during case 2.

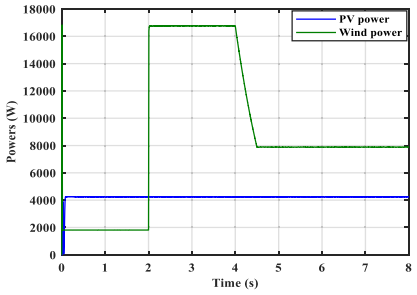

FIGURE 31. Optimum generated power from PV and WG systems at case 2.

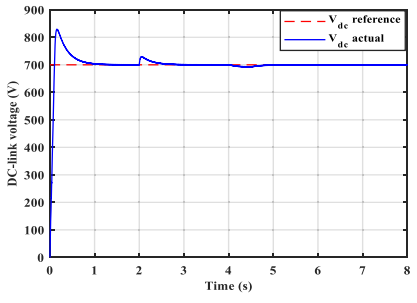

FIGURE 32. Reference and actual DC-link voltage response during case 2.

focus on the output from these two controllers. To achieve this comparison, a constant wind speed of 6 m/s and constant radiation of 1000 kWh/m^2 is adopted. The tuning gains used for all PI controllers used in GSC, MSC, and IC are presented in Tables 3, 4, and 5 respectively. Figure 13 shows the optimum and actual wind power coefficient while Fig. 14 illustrates

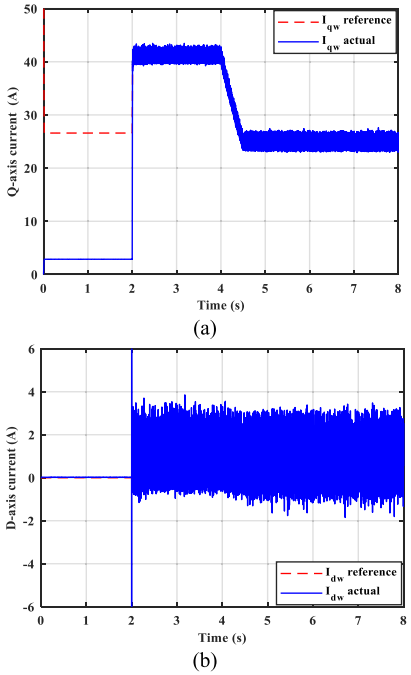

FIGURE 33. DQ-axis currents generated from the WGS during case 2. (a) q-axis for actual and reference values, and (b) d-axis for actual and reference values.

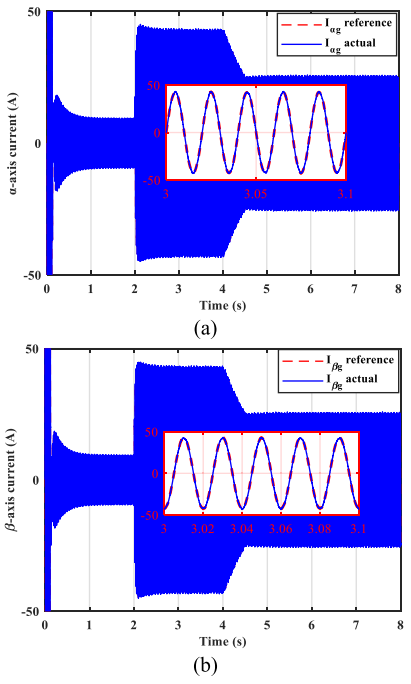

FIGURE 34. Injected currents into the grid during case 2. (a) α-axis for actual and reference values, and (b) β-axis for actual and reference values.

the reference and actual DC-link voltage response under the use of the MPC and PI-based SVM. It can be noticed that the PI controller tracks the optimum power very well compared to the use of MPC beside a smaller overshot in the DC-link voltage. On the other hand, the MPC can achieve lower current variations on the d- and q-axis of the generator current

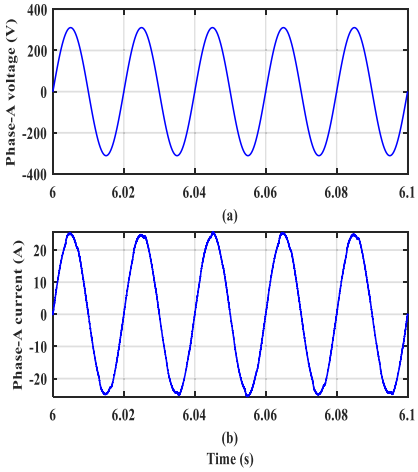

FIGURE 35. Simulation results of the main grid during case 2. (a) Phase-A voltage, and (b) Phase-A current.

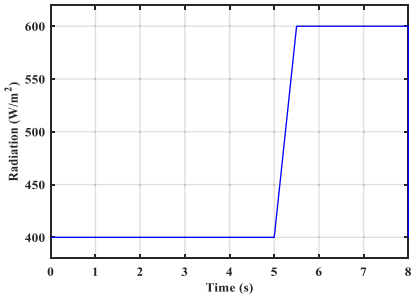

FIGURE 36. Solar radiation profile during case 3.

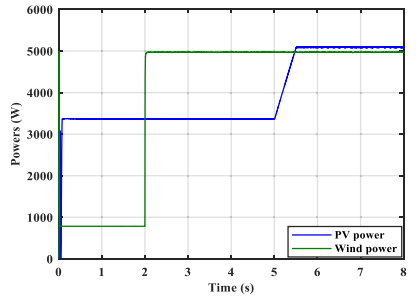

FIGURE 37. Optimum generated power from PV and WG systems at case 3.

compared to SVM as depicted in Figs. 15 and 16 respectively. This reduction in the current variation reduces the developed torque and hence increases the generator lifetime. In addition, the use of MPC leads to lower current distortion in the injected current to the grid as illustrated by the $\alpha\beta$-axis currents shown in Figs. 17 and 18.

B. CASE 2: FIXED RADIATION AND FIXED WIND SPEED

The MPC is used to assess the potential of the proposed HRESs using a rated value of solar radiation of 1000 kWh/m^2 and a fixed value of wind speed of 8 m/s, which is normal in most places. Because the system is connected to the grid and not an isolated load, there are no restrictions on the amount

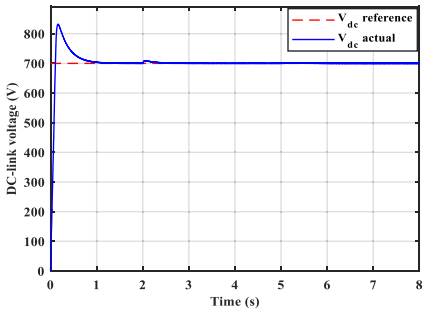

FIGURE 38. Reference and actual DC-link voltage response during case 3.

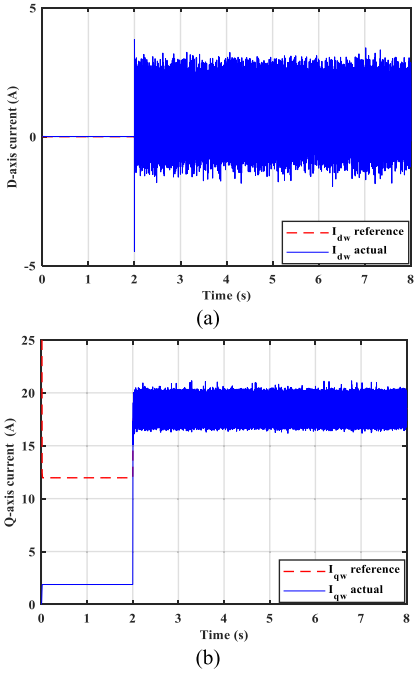

FIGURE 39. DQ-axis currents generated from the WGS during case 3. (a) d-axis for actual and reference values, and (b) q-axis for actual and reference values.

of generated power that can be sent to the grid, and so the entire generated power will be sent to the grid. The PV injects power from the starting as it is static generation. Meanwhile, the wind generating system injects power to the grid after 2 s till the generator reaches to steady state and overcomes the inertia. Figure 19 shows the amount of generated power from both the PV system and WGS. After 2 seconds, the actual wind power coefficient closely follows the optimal one, as seen in Fig. 20. As shown in Fig. 21, the value of the Q-axis current generated by the WGS closely reflects the reference value responsible for producing the maximum power from the wind.

Meanwhile, the reference value for the d-axis current is zero to reduce the loss. The actual value tracks this reference value very well, as confirmed from Fig. 22. Figure 23 shows the DC-link voltage regulated to be constant through the grid side converter aided with the PI controller. Further, the MPC is used to regulate the injected current to the grid where the

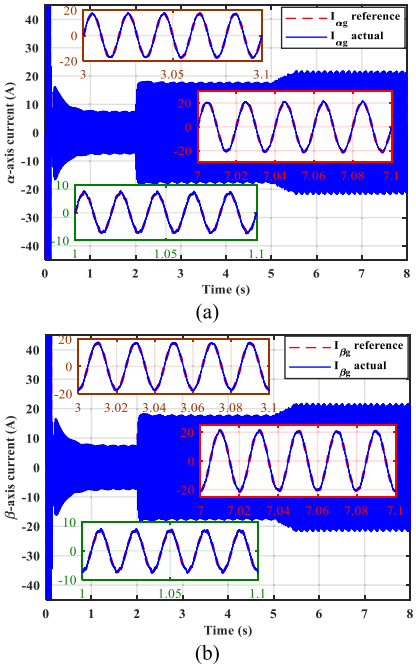

FIGURE 40. Injected currents into the grid during case 3. (a) α-axis for actual and reference values, and (b) β-axis for actual and reference values.

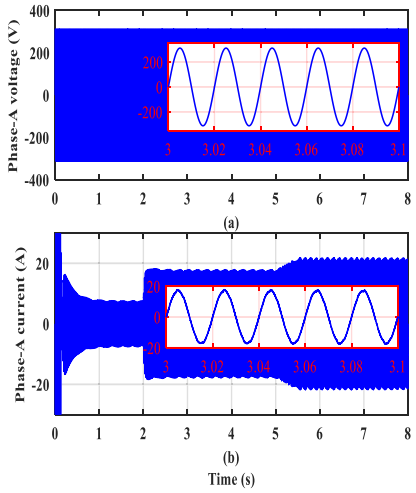

FIGURE 41. Simulation results of the main grid during case 3. (a) Phase-A voltage, and (b) Phase-A current.

actual values of the $\alpha\beta$-axis current track their references value very well, as seen in Figs. 24 and 25. Finally, the phase-A voltage and current are shown in Fig. 26-a and b, respectively. It is observed that the control succeeded in achieving the unity power factor.

C. CASE 3: WIND SPEED VARIATION AND CONSTANT RADIATION

The effect of wind speed fluctuation and constant radiation on the control and overall HRES is investigated in this scenario. The radiation level is set to 500 W/m^2, and the wind speed profile is depicted in Fig. 27. Figures 28 and 29 show the average output PV voltage and current, confirming that

the MPC extracts the MPP from the PV panels successfully. Meanwhile, the MPP from the wind generating system is proven by Fig. 30, which shows the MPC's ability to extract MPP at various wind speeds. The optimal quantity of the generated power from both PV and WGS is shown in Fig. 31. The reference and the actual DC-link voltage values is shown in Fig. 32. It is noticed that the actual value tracks the reference value but with a disturbance at wind speed changes. Figure 33-a and b represent the reference and the actual dq-axis currents to extract the MPP from the WGS, where the MPC ensures that the actual values follow the reference values with a good transient. Regarding the grid side inverter control, the injected current valuesIt is confirmed from Figs. 34-a and b, the actual values match very well with the reference values. Also, the unity power factor is confirmed from the phase-A voltage and current where both are in-phase, as shown in Figs. 35-a and b.

D. CASE 4: SOLAR RADIATION VARIATION AND CONSTANT WIND SPEED

This scenario is offered to check the variability of solar radiation and fixed wind speed for further testing of the MPC and the overall system. The wind speed is kept constant at 6m/s while the solar radiation, shown in Fig. 36, increases from 400 to 600 W/m^2. Figure 37 demonstrates the optimal generated wind and PV power where the wind-generated power remains constant at the optimum value and the PV output power changes in response to the PV radiation. The DC-bus voltage is regulated at the reference value as shown in Fig. 38. This demonstrates the MPC controller's capacity to control MPP in WGS and PV systems in which the actual values of the DQ-axis current generated from the wind follow the reference one as reported in Figs. 39-a and b.

Meanwhile, the MPC for the grid side converter is working well, as proven from responses $\alpha\beta$-axis of the grid currents, and also Phase-A grid voltage and current as shown in Figs. 40 and 41, respectively. It is observed that the injected current increases with the increase of solar radiation.

The main findings of the results can be summarized as follows.

- MPC is comparable to traditional control methods, and it generally outperforms them in terms of flexibility and performance.
- The main driver for tackling real-world issues in the field of power electronics is the flexibility of the proposed MPC technology.
- Under a variety of model uncertainties, voltage prediction and the steady-state performance of the proposed control method are enhanced.
- The reference current can be correctly and quickly tracked using the suggested MPC approach, which also exhibits good steady state and dynamic performance. The suggested MPC has the highest steady-state performance.
- In the majority of instances of model mismatches, the performance degradation of the suggested control system is minimal and acceptable given the current measurement error.
- The suggested control method is adaptable to various cost functions; as a result, it is superior in terms of real hardware implementation.
- It has been established through analysis of the grid current THD that the proposed method is more resistant to grid variation than the PI control strategy.
- The high-order harmonics of the output current can be realised by the suggested MPC algorithm, which is advantageous for the filter design.
- When compared to the traditional PI control scheme, the suggested FCS-MPC control method operates well, has good tracking capability, rejects disturbances, and responds more quickly.
- This method's application requires fewer computational resources.
- The MPC algorithm that is being given has reduced sensitivity to the filter settings.
- The suggested solution directly incorporates MPC results, which are simple to include in DSP controller.

The suggested control strategy has a simpler structure than standard approaches that employ classical controllers, making it easier to implement and tune.

VI. CONCLUSION

This research shows that the finite-control-set MPC linked with a hybrid PV/WT-powered microgrid improves the performance of the grid-connected systems. Maximum power extraction is accomplished for both PVs by implementing the IC algorithm-based MPC for the PV system. In addition, the FCS-MPC is used to extract the MPP from the wind generating system. The DC-bus voltage is regulated along with the FCS-MPC to achieve the unity power factor through the three-phase grid-connected inverter. The proposed system was simulated in the following four scenarios: Case I: a comparative analysis of the outcomes between MPC and contemporary PI based SVM. Case II: during both fixed wind speed and radiation, the optimal power produced by the hybrid system under 1000kWh/m^2 of irradiation for 8kW and 8m/s of wind speed to create 12kW is shown. The suggested machine controller ensures the optimal wind power output based on simulation findings by keeping the power coefficient at the reference value and regulating the DC-bus voltage. In Case III: variable wind speed and fixed irradiance, the WT's dynamic performance is examined by maintaining constant irradiance. At a rate of 4 s, the wind speed is reduced from 9 m/s to 7 m/s, but a low irradiance of 500 W/m^2 is maintained for PV panels. The simulation validated the anticipated case II's dynamic response. Situation IV: variable irradiance and fixed wind speed is another dynamic case in which the IC-based MPC was developed and followed the maximum power. In each case mentioned earlier, the three-phase inverter references and phase currents indicate that the suggested system is more precise than the current PI. The

voltage of the DC-bus was controlled to be almost equal to the reference voltages.

ACKNOWLEDGMENT

The authors would like to thank the support of Prince Sultan University for paying the Article Processing Charges (APC) of this publication.

REFERENCES

[1] Y. Shan, J. Hu, K. W. Chan, Q. Fu, and J. M. Guerrero, "Model predictive control of bidirectional DC–DC converters and AC/DC interlinking converters—A new control method for PV-wind-battery microgrids," *IEEE Trans. Sustain. Energy*, vol. 10, no. 4, pp. 1823–1833, Oct. 2019, doi: 10.1109/TSTE.2018.2873390.

[2] I. Jamal, M. F. Elmorshedy, S. M. Dabour, E. M. Rashad, W. Xu, and D. J. Almakhles, "A comprehensive review of grid-connected PV systems based on impedance source inverter," *IEEE Access*, vol. 10, pp. 89101–89123, 2022, doi: 10.1109/ACCESS.2022.3200681.

[3] J. Schiffer, T. Seel, J. Raisch, and T. Sezi, "Voltage stability and reactive power sharing in inverter-based microgrids with consensus-based distributed voltage control," *IEEE Trans. Control Syst. Technol.*, vol. 24, no. 1, pp. 96–109, Jan. 2016, doi: 10.1109/TCST.2015.2420622.

[4] Y.-J. Lee, A. Khaligh, and A. Emadi, "Advanced integrated bidirectional AC/DC and DC/DC converter for plug-in hybrid electric vehicles," *IEEE Trans. Veh. Technol.*, vol. 58, no. 8, pp. 3970–3980, Oct. 2009, doi: 10.1109/TVT.2009.2028070.

[5] A. Emadi and M. Ehsani, "Multi-converter power electronic systems: Definition and applications," in *Proc. IEEE 32nd Annu. Power Electron. Specialists Conf.*, vol. 2, 2001, pp. 1230–1236, doi: 10.1109/PESC.2001.954287.

[6] H. van Hoek, M. Boesing, D. van Treek, T. Schoenen, and R. W. De Doncker, "Power electronic architectures for electric vehicles," in *Proc. Emobility Electr. Power Train*, 2010, pp. 1–6, doi: 10.1109/EMOBILITY.2010.5668048.

[7] M. Elsied, A. Salem, A. Oukaour, H. Gualous, H. Chaoui, F. T. Youssef, D. Belie, J. Melkebeek, and O. Mohammed, "Efficient power-electronic converters for electric vehicle applications," in *Proc. IEEE Vehicle Power Propuls. Conf. (VPPC)*, Oct. 2015, pp. 1–6, doi: 10.1109/VPPC.2015.7352941.

[8] S. Kutter and B. Baker, "Predictive online control for hybrids: Resolving the conflict between global optimality, robustness and real-time capability," in *Proc. IEEE Vehicle Power Propuls. Conf.*, Sep. 2010, pp. 1–7, doi: 10.1109/VPPC.2010.5729231.

[9] J. Unger, M. Kozek, and S. Jakubek, "Nonlinear model predictive energy management controller with load and cycle prediction for non-road HEV," *Control Eng. Pract.*, vol. 36, pp. 120–132, Mar. 2015, doi: 10.1016/j.conengprac.2014.12.001.

[10] S. Richter, S. Mariethoz, and M. Morari, "High-speed online MPC based on a fast gradient method applied to power converter control," in *Proc. Amer. Control Conf.*, Jun. 2010, pp. 4737–4743, doi: 10.1109/ACC.2010.5531095.

[11] P. Cortes, M. P. Kazmierkowski, R. M. Kennel, D. E. Quevedo, and J. Rodriguez, "Predictive control in power electronics and drives," *IEEE Trans. Ind. Electron.*, vol. 55, no. 12, pp. 4312–4324, Dec. 2008, doi: 10.1109/TIE.2008.2007480.

[12] P. Karamanakos, T. Geyer, N. Oikonomou, F. D. Kieferndorf, and S. Manias, "Direct model predictive control: A review of strategies that achieve long prediction intervals for power electronics," *IEEE Ind. Electron. Mag.*, vol. 8, no. 1, pp. 32–43, Mar. 2014, doi: 10.1109/MIE.2013.2290474.

[13] D. E. Quevedo, R. P. Aguilera, M. A. Perez, and P. Cortes, "Finite control set MPC of an AFE rectifier with dynamic references," in *Proc. IEEE Int. Conf. Ind. Technol.*, Mar. 2010, pp. 1265–1270, doi: 10.1109/ICIT.2010.5472621.

[14] S. Mariethoz and M. Morari, "Explicit model-predictive control of a PWM inverter with an LCL filter," *IEEE Trans. Ind. Electron.*, vol. 56, no. 2, pp. 389–399, Feb. 2009, doi: 10.1109/TIE.2008.2008793.

[15] Z. Zhang and R. Kennel, "Direct model predictive control of three-level NPC back-to-back power converter PMSG wind turbine systems under unbalanced grid," in *Proc. IEEE Int. Symp. Predictive Control Electr. Drives Power Electron. (PRECEDE)*, Oct. 2015, pp. 97–102, doi: 10.1109/PRECEDE.2015.7395590.

[16] J. Rodriguez, J. Pontt, P. Correa, P. Lezana, and P. Cortes, "Predictive power control of an AC/DC/AC converter," in *Proc. Fourtieth IAS Annu. Meeting. Conf. Rec. Ind. Appl. Conf.*, 2005, pp. 934–939, doi: 10.1109/IAS.2005.1518458.

[17] Y. Gu, X. Xiang, W. Li, and X. He, "Mode-adaptive decentralized control for renewable DC microgrid with enhanced reliability and flexibility," *IEEE Trans. Power Electron.*, vol. 29, no. 9, pp. 5072–5080, Sep. 2014, doi: 10.1109/TPEL.2013.2294204.

[18] S. Mariéthoz, A. Fuchs, and M. Morari, "A VSC-HVDC decentralized model predictive control scheme for fast power tracking," *IEEE Trans. Power Del.*, vol. 29, no. 1, pp. 462–471, Feb. 2014, doi: 10.1109/TPWRD.2013.2265277.

[19] J. Hu, Y. Xu, K. W. Cheng, and J. M. Guerrero, "A model predictive control strategy of PV-battery microgrid under variable power generations and load conditions," *Appl. Energy*, vol. 221, pp. 195–203, Jul. 2018, doi: 10.1016/j.apenergy.2018.03.085

[20] E. Hossain, R. Perez, A. Nasiri, and S. Padmanaban, "A comprehensive review on constant power loads compensation techniques," *IEEE Access*, vol. 6, pp. 33285–33305, 2018, doi: 10.1109/ACCESS.2018.2849065.

[21] S. C. Smithson and S. S. Williamson, "Constant power loads in more electric vehicles—An overview," in *Proc. 38th Annu. Conf. IEEE Ind. Electron. Soc. (IECON)*, Oct. 2012, pp. 2914–2922, doi: 10.1109/IECON.2012.6389432.

[22] Z. Zhang, F. Wang, T. Sun, J. Rodriguez, and R. Kennel, "FPGA-based experimental investigation of a quasi-centralized model predictive control for back-to-back converters," *IEEE Trans. Power Electron.*, vol. 31, no. 1, pp. 662–674, Jan. 2016, doi: 10.1109/TPEL.2015.2397695.

[23] F. Grimm and Z. Zhang, "Centralized direct model predictive control of Back-to-Back converters," in *Proc. IEEE Int. Power Electron. Appl. Conf. Exposit. (PEAC)*, Nov. 2018, pp. 1–6, doi: 10.1109/PEAC.2018.8590424.

[24] C. Jiang, Z. Quan, D. Zhou, and Y. Li, "A centralized CB-MPC to suppress low-frequency ZSCC in modular parallel converters," *IEEE Trans. Ind. Electron.*, vol. 68, no. 4, pp. 2760–2771, Apr. 2021, doi: 10.1109/TIE.2020.2982111.

[25] T. Hausberger, A. Kugi, A. Eder, and W. Kemmetmuller, "Cooperative model predictive control concepts for coupled AC/DC-and DC/DC-power converters," *IEEE Trans. Control Syst. Technol.*, early access, Jun. 13, 2022, doi: 10.1109/TCST.2022.3179583.

[26] A. N. Venkat, J. B. Rawlings, and S. J. Wright, "Stability and optimality of distributed model predictive control," in *Proc. 44th IEEE Conf. Decis. Control*, Dec. 2005, pp. 6680–6685, doi: 10.1109/CDC.2005.1583235.

[27] A. N. Venkat, I. A. Hiskens, J. B. Rawlings, and S. J. Wright, "Distributed MPC strategies with application to power system automatic generation control," *IEEE Trans. Control Syst. Technol.*, vol. 16, no. 6, pp. 1192–1206, Nov. 2008, doi: 10.1109/TCST.2008.919414.

[28] D. K. Molzahn, F. Dörfler, H. Sandberg, S. H. Low, S. Chakrabarti, R. Baldick, and J. Lavaei, "A survey of distributed optimization and control algorithms for electric power systems," *IEEE Trans. Smart Grid*, vol. 8, no. 6, pp. 2941–2962, 2017, doi: 10.1109/TSG.2017.2720471.

[29] A. Parisio, C. Wiezorek, T. Kyntäjä, J. Elo, K. Strunz, and K. H. Johansson, "Cooperative MPC-based energy management for networked microgrids," *IEEE Trans. Smart Grid*, vol. 8, no. 6, pp. 3066–3074, Nov. 2017, doi: 10.1109/TSG.2017.2726941.

[30] Y. Zheng, J. Zhou, Y. Xu, Y. Zhang, and Z. Qian, "A distributed model predictive control based load frequency control scheme for multi-area interconnected power system using discrete-time Laguerre functions," *ISA Trans.*, vol. 68, pp. 127–140, May 2017, doi: 10.1016/j.isatra.2017.03.009.

[31] M. Ma, H. Chen, X. Liu, and F. Allgöwer, "Distributed model predictive load frequency control of multi-area interconnected power system," *Int. J. Electr. Power Energy Syst.*, vol. 62, pp. 289–298, Nov. 2014, doi: 10.1016/j.ijepes.2014.04.050.

[32] P. McNamara, R. R. Negenborn, B. De Schutter, and G. Lightbody, "Optimal coordination of a multiple HVDC link system using centralized and distributed control," *IEEE Trans. Control Syst. Technol.*, vol. 21, no. 2, pp. 302–314, Mar. 2013, doi: 10.1109/TCST.2011.2180906.

[33] L. Tarisciotti, G. Lo Calzo, A. Gaeta, P. Zanchetta, F. Valencia, and D. Saez, "A distributed model predictive control strategy for back-to-back converters," *IEEE Trans. Ind. Electron.*, vol. 63, no. 9, pp. 5867–5878, Sep. 2016, doi: 10.1109/TIE.2016.2527693.

[34] S. Vazquez, J. Rodriguez, M. Rivera, L. G. Franquelo, and M. Norambuena, "Model predictive control for power converters and drives: Advances and trends," *IEEE Trans. Ind. Electron.*, vol. 64, no. 2, pp. 935–947, Nov. 2017, doi: 10.1109/TIE.2016.2625238.

[35] T. Hausberger, A. Kugi, A. Eder, and W. Kemmetmüller, "High-speed nonlinear model predictive control of an interleaved switching DC/DC-converter," *Control Eng. Pract.*, vol. 103, Oct. 2020, Art. no. 104576, doi: 10.1016/j.conengprac.2020.104576.
[36] *SunPower*, SunPower Corp., CA, USA, 1985. [Online]. Available: https://us.sunpower.com/company
[37] K. M. Kotb, M. F. Elmorshedy, H. S. Salama, and A. Dán, "Enriching the stability of solar/wind DC microgrids using battery and superconducting magnetic energy storage based fuzzy logic control," *J. Energy Storage*, vol. 45, Jan. 2022, Art. no. 103751.
[38] A. Maleki, H. Hafeznia, M. A. Rosen, and F. Pourfayaz, "Optimization of a grid-connected hybrid solar-wind-hydrogen CHP system for residential applications by efficient metaheuristic approaches," *Appl. Thermal Eng.*, vol. 123, pp. 1263–1277, Aug. 2017, doi: 10.1016/j.applthermaleng.2017.05.100.
[39] *Wind Energy Solution*.
[40] W. Zhang, A. Maleki, and M. A. Rosen, "A heuristic-based approach for optimizing a small independent solar and wind hybrid power scheme incorporating load forecasting," *J. Cleaner Prod.*, vol. 241, Dec. 2019, Art. no. 117920, doi: 10.1016/J.JCLEPRO.2019.117920.
[41] A. T. Dahiru and C. W. Tan, "Optimal sizing and techno-economic analysis of grid-connected nanogrid for tropical climates of the savannah," *Sustain. Cities Soc.*, vol. 52, Jan. 2020, Art. no. 101824, doi: 10.1016/J.SCS.2019.101824.
[42] U. Yilmaz, O. Turksoy, and A. Teke, "Improved MPPT method to increase accuracy and speed in photovoltaic systems under variable atmospheric conditions," *Int. J. Electr. Power Energy Syst.*, vol. 113, pp. 634–651, Dec. 2019, doi: 10.1016/j.ijepes.2019.05.074.
[43] T. Noguchi, S. Togashi, and R. Nakamoto, "Short-current pulse-based maximum-power-point tracking method for multiple photovoltaic-and-converter module system," *IEEE Trans. Ind. Electron.*, vol. 49, no. 1, pp. 217–223, Feb. 2002, doi: 10.1109/41.982265.
[44] M. A. S. Masoum, H. Dehbonei, and E. F. Fuchs, "Theoretical and experimental analyses of photovoltaic systems with voltage and current-based maximum power point trackin," *IEEE Trans. Energy Convers.*, vol. 19, no. 3, pp. 652–653, Sep. 2004, doi: 10.1109/TEC.2004.832449.
[45] H. Mahamudul, M. Saad, and M. Ibrahim Henk, "Photovoltaic system modeling with fuzzy logic based maximum power point tracking algorithm," *Int. J. Photoenergy*, vol. 2013, pp. 1–10, Sep. 2013, doi: 10.1155/2013/762946.
[46] B. Bendib, H. Belmili, and F. Krim, "A survey of the most used MPPT methods: Conventional and advanced algorithms applied for photovoltaic systems," *Renew. Sustain. Energy Rev.*, vol. 45, pp. 637–648, May 2015, doi: 10.1016/j.rser.2015.02.009.
[47] C. P. Roy, D. Vijaybhaskar, and T. Maity, "Modelling of fuzzy logic controller for variable-step MPPT in photovoltaic system," in *Proc. IEEE 1st Int. Conf. Condition Assessment Techn. Electr. Syst. (CATCON)*, Dec. 2013, pp. 341–346, doi: 10.1109/CATCON.2013.6737524.
[48] A. Safari and S. Mekhilef, "Simulation and hardware implementation of incremental conductance MPPT with direct control method using Cuk converter," *IEEE Trans. Ind. Electron.*, vol. 58, no. 4, pp. 1154–1161, Apr. 2011, doi: 10.1109/TIE.2010.2048834.
[49] A. Dahbi, N. Nait-Said, and M.-S. Nait-Said, "A novel combined MPPT-pitch angle control for wide range variable speed wind turbine based on neural network," *Int. J. Hydrogen Energy*, vol. 41, no. 22, pp. 9427–9442, 2016, doi: 10.1016/j.ijhydene.2016.03.105.
[50] S. M. Muyeen, A. Al-Durra, and J. Tamura, "Variable speed wind turbine generator system with current controlled voltage source inverter," *Energy Convers. Manage.*, vol. 52, no. 7, pp. 2688–2694, Jul. 2011, doi: 10.1016/j.enconman.2011.02.001.
[51] F. Delfino, F. Pampararo, R. Procopio, and M. Rossi, "A feedback linearization control scheme for the integration of wind energy conversion systems into distribution grids," *IEEE Syst. J.*, vol. 6, no. 1, pp. 85–93, Mar. 2012, doi: 10.1109/JSYST.2011.2163002.
[52] M. Karabacak, "A new perturb and observe based higher order sliding mode MPPT control of wind turbines eliminating the rotor inertial effect," *Renew. Energy*, vol. 133, pp. 807–827, Apr. 2019, doi: 10.1016/j.renene.2018.10.079.
[53] H. Fathabadi, "Maximum mechanical power extraction from wind turbines using novel proposed high accuracy single-sensor-based maximum power point tracking technique," *Energy*, vol. 113, pp. 1219–1230, Oct. 2016, doi: 10.1016/j.energy.2016.07.081.
[54] O. Turksoy, S. Ayasun, Y. Hames, and S. Sonmez, "Gain-phase margins-based delay-dependent stability analysis of pitch control system of large wind turbines," *Trans. Inst. Meas. Control*, vol. 41, no. 13, pp. 3626–3636, Sep. 2019, doi: 10.1177/0142331219834605.
[55] O. Turksoy, S. Ayasun, Y. Hames, and S. Sonmez, "Computation of robust PI-based pitch controller parameters for large wind turbines," *Can. J. Electr. Comput. Eng.*, vol. 43, no. 1, pp. 57–63, 2020, doi: 10.1109/CJECE.2019.2923050.
[56] M. F. Elmorshedy, S. M. Allam, A. I. A. Shobair, and E. M. Rashad, "Voltage and frequency control of a stand-alone wind-energy conversion system based on PMSG," in *Proc. 4th Int. Conf. Electric Power Energy Convers. Syst. (EPECS)*, Nov. 2015, pp. 1–6, doi: 10.1109/EPECS.2015.7368494.
[57] M. F. Elmorshedy, M. R. Islam, M. M. Ali, F. F. M. El-Sousy, and M. M. Amin, "Improved standalone PMSG based wind-generating system using MPPT and MRAS for speed estimation," in *Proc. IEEE 4th Int. Conf. Comput., Power Commun. Technol. (GUCON)*, Sep. 2021, pp. 1–6, doi: 10.1109/GUCON50781.2021.9573906.
[58] K. Palanimuthu, G. Mayilsamy, S. R. Lee, S. Y. Jung, and Y. H. Joo, "Comparative analysis of maximum power extraction and control methods between PMSG and PMVG-based wind turbine systems," *Int. J. Electr. Power Energy Syst.*, vol. 143, Dec. 2022, Art. no. 108475.
[59] M. F. Elmorshedy, S. M. Allam, and E. M. Rashad, "Load voltage control and maximum power extraction of a stand-alone wind-driven PMSG including unbalanced operating conditions," in *Proc. 18th Int. Middle East Power Syst. Conf. (MEPCON)*, Dec. 2016, pp. 552–559, doi: 10.1109/MEPCON.2016.7836946.
[60] P. Das, M. Abdelrahem, A. Farhan, M. A. Ismeil, and R. Kennel, "Predictive direct torque control of permanent magnet synchronous generators (PMSGs) without weighting factors," in *Proc. IEEE Conf. Power Electron. Renew. Energy (CPERE)*, Oct. 2019, pp. 296–301, doi: 10.1109/CPERE45374.2019.8980112.
[61] N. Mughees, M. H. Jaffery, and M. Jawad, "A new predictive control strategy for improving operating performance of a permanent magnet synchronous generator-based wind energy and superconducting magnetic energy storage hybrid system integrated with grid," *J. Energy Storage*, vol. 55, Nov. 2022, Art. no. 105515.
[62] Y. Liang, Y. He, and Y. Niu, "Robust errorless-control-targeted technique based on MPC for microgrid with uncertain electric vehicle energy storage systems," *Energies*, vol. 15, no. 4, p. 1398, Feb. 2022.
[63] Q. Xing, Z. Zhang, T. Dragicevic, and J. Rodriguez, "Bias-free predictive control of power converters with LCL-filter in micro-energy systems," *IEEE Trans. Ind. Electron.*, early access, Aug. 16, 2022, doi: 10.1109/TIE.2022.3196360.

MAHMOUD F. ELMORSHEDY (Member, IEEE) was born in Gharbeya, Egypt, in 1989. He received the B.Sc. and M.Sc. degrees in electrical engineering from Tanta University, Egypt, in 2012 and 2016, respectively, and the Ph.D. degree in electrical engineering from the School of Electrical and Electronic Engineering, Huazhong University of Science and Technology, China, in 2020. He started working as a Teaching Assistant with the Department of Electrical Power and Machines Engineering, Faculty of Engineering, Tanta University, in 2013, where he was promoted to an Assistant Lecturer, in June 2016. He is currently working as an Assistant Professor (On academic leave) with the Department of Electrical Power and Machines Engineering, Faculty of Engineering, Tanta University. He is also a Postdoctoral Fellow with the Renewable Energy Laboratory, College of Engineering, Prince Sultan University, Riyadh, Saudi Arabia. His research interests include linear induction motor, predictive control, power electronics, and renewable energy.

HABIB UR RAHMAN HABIB (Senior Member, IEEE) received the B.Sc. degree in electrical engineering and the M.Sc. degree in electrical power engineering from the University of Engineering and Technology Taxila, Pakistan, in 2009 and 2015, respectively, and the Ph.D. degree in electrical engineering from the State Key Laboratory of Advanced Electromagnetic Engineering, School of Electrical and Electronics Engineering, Huazhong University of Science and Technology, Wuhan, China, in 2021.

Since 2009, he has been with the COMSATS Institute of Information Technology, Pakistan, and the Wah Engineering College, University of Wah, Pakistan. He has been a Management Trainee Officer (Maintenance Department) with Dynamic Packaging Pvt. Ltd., Lahore, Pakistan. He is currently with the Department of Electrical Engineering, University of Engineering and Technology Taxila. His research interests include microgrid, smart grid, energy economics, control applications in power systems, renewable resources integration, power electronics applications to power systems, and distributed generation. He has been serving as a Reviewer for many journals, including IEEE Systems Journal, *International Transactions on Electrical Energy Systems*, IEEE Access, and *International Journal of Power Electronics and Drive Systems*. He is also a member of many technical and professional committees, including IEEE. He has participated in different international conferences including Singapore, China, USA, Pakistan, Dubai, United Arab Emirates, and Australia. He is a HEC approved Ph.D. Supervisor. He is also working on university—industry linkages and academic engagements in promoting technology transfer and stimulating student employability.

MOSAAD M. ALI was born in Kafr El-Shaikh, Egypt, in 1988. He received the M.Sc. degree in electrical engineering from Alexandria University, Egypt, in 2017, and the Ph.D. degree from the State Key Laboratory of Advanced Electromagnetic Engineering and Technology, Huazhong University of Science and Technology, China. He has been working as a Teaching Assistant at the Department of Electrical Engineering, Faculty of Engineering, Kafrelsheikh University, since 2012. In September 2021, he was promoted to the degree of an Assistant Professor with the Department of Electrical Engineering. His research interests include linear induction motor, sliding mode control, and renewable energy.

M. JAGABAR SATHIK (Senior Member, IEEE) received the B.Eng. degree in electronics and communication engineering from Madurai Kamaraj University, Madurai, India, in 2002, and the M.Eng. and Ph.D. degrees from the Faculty of Electrical Engineering, Anna University, Chennai, India, in 2004 and 2016, respectively. He is currently an Associate Professor with the Department of Electrical and Electronics Engineering, SRM Institute of Science and Technology, Chennai. He is currently a Postdoctoral Fellow with the Renewable Energy Laboratory, College of Engineering, Prince Sultan University, Riyadh, Saudi Arabia. He was a consultant of various power electronics companies for the design of power electronics converters. He has authored more than 60 articles publications in international refereed journals and conference proceedings. His current research interests include multilevel inverters, grid-connected inverters, and power electronics converters and its applications to renewable energy systems. He received the certificate of recognition from IEEE Madras Section for paper published (2019–2021). He is serving as a Regular Reviewer for several journals, including the IEEE Transactions on Power Electronics, the IEEE Transactions on Industrial Electronics, the IEEE Journal of Emerging and Selected Topics in Power Electronics, and the *IET Power Electronics*.

DHAFER J. ALMAKHLES (Senior Member, IEEE) received the B.E. degree in electrical engineering from the King Fahd University of Petroleum and Minerals, Dhahran, Saudi Arabia, in 2006, and the master's (Hons.) and Ph.D. degrees from The University of Auckland, New Zealand, in 2011 and 2016, respectively. Since 2016, he has been with Prince Sultan University, Saudi Arabia, where he is currently the Chairperson of the Communications and Networks Engineering Department and the Director of the Science and Technology Unit. He is also the Leader of the Renewable Energy Research Team and the Laboratory, Prince Sultan University. His research interests include the hardware implementation of control theory, signal processing, networked control systems, and sliding mode.